nature COMMUNICATIONS

ARTICLE

Received 24 Jul 2012 | Accepted 31 Oct 2012 | Published 27 Nov 2012

DOI: 10.1038/ncomms2242

Non-syngas direct steam reforming of methanol to hydrogen and carbon dioxide at low temperature

Kai Man Kerry Yu[1,*], Weiyi Tong[1,2,*], Adam West[1], Kevin Cheung[1], Tong Li[3], George Smith[3], Yanglong Guo[2] & Shik Chi Edman Tsang[1]

A non-syngas direct steam reforming route is investigated for the conversion of methanol to hydrogen and carbon dioxide over a $CuZnGaO_x$ catalyst at 150–200 °C. This route is in marked contrast with the conventional complex route involving steam reformation to syngas (CO/H_2) at high temperature, followed by water gas shift and CO cleanup stages for hydrogen production. Here we report that high quality hydrogen and carbon dioxide can be produced in a single-step reaction over the catalyst, with no detectable CO (below detection limit of 1 ppm). This can be used to supply proton exchange membrane fuel cells for mobile applications without invoking any CO shift and cleanup stages. The working catalyst contains, on average, 3–4 nm copper particles, alongside extremely small size of copper clusters stabilized on a defective $ZnGa_2O_4$ spinel oxide surface, providing hydrogen productivity of 393.6 ml g^{-1}-cat h^{-1} at 150 °C.

[1] Wolfson Catalysis Centre, Department of Chemistry, University of Oxford, South Parks Road, Oxford, OX1 3QR, UK. [2] Research Institute of Industrial Catalysis, East China University of Science & Technology, Shanghai 200237, China. [3] Department of Materials, University of Oxford, Parks Road, Oxford OX1 3PH, UK. * These authors equally contributed to this work. Correspondence and requests for materials should be addressed to E.T. (email:edman.tsang@chem.ox.ac.uk).

Global efforts are currently underway to minimize the emissions of NO_x, SO_x, hydrocarbons, CO and CO_2. The use of hydrogen as an environmentally-friendly energy carrier has been massively encouraged in recent years. Hydrogen is considered to be the best fuel vector as emissions are non-polluting and it offers high efficiency when used in proton exchange membrane (PEM) fuel cells. For portable applications such as cell phones, mp3-players, laptop computers and similar niche products, PEM fuel cells are deemed to be more energy efficient than battery technology.[1] Low temperature micro-PEM fuel cells and micro fabrication technologies are potentially the preferred choices for these consumer products. There are a number of ways of obtaining hydrogen from both renewable and non-renewable sources on a large industrial scale, but the storage and transfer of hydrogen in solid systems for mobile use is problematic owing to poor volumetric and weight energy densities.[2] In addition, ultra-pure hydrogen gas is required by PEM fuel cells. In particular, the gas stream has to be free from CO (<10 ppm), otherwise the catalytic performance of the fuel cell is significantly degraded.[3] The use of *in-situ* reforming of organic compounds with downstream multistage CO post-treatments such as the water gas shift (WGS) reaction, selective oxidation of CO to CO_2, hydrogenation of CO to methane or membrane technology, and so on, is not applicable. This is because these cumbersome multistage processes commonly take place at elevated temperatures, which precludes their adaptation in the small portable devices where space and heat management are at a premium.

Hydrogen stored in a chemical form as liquid organic compounds and released *in situ* on demand at low temperature without CO contamination appears to be a more promising direction for mobile fuel cells. The primary liquid fuel can be stored in a disposable or recyclable cartridge, which is replaceable and logistically feasible. The generation of hydrogen from formic acid, which is non-toxic and liquid at room temperature, with a density of 1.22 g ml^{-1}, has recently been demonstrated.[4] On the other hand, the direct use of methanol, which is a key platform chemical for existing fuel and chemical infrastructures, and which has a high energy content of 5,420 kcal kg^{-1}, is economically more attractive.[5,6] Although methanol is currently produced industrially from non-renewable fuels over $Cu/ZnO/Al_2O_3$ catalysts,[7–9] the *in-situ* production of hydrogen from methanol facilitates efficient on-site energy conversion and cleaner emissions and is therefore potentially an attractive process. Methanol can also be synthesized by CO_2 hydrogenation, and may be used for future recycling of CO_2 to fuel, if renewable hydrogen from water can be made available.[10]

Direct catalytic hydrogen production by the low temperature steam reformation process with no co-production of CO gas at low temperature is described by equation (1) below:

$$CH_3OH + H_2O \rightarrow CO_2 + 3H_2 \rightarrow \Delta H^o = +49\ kJ\ mol^{-1} \quad (1)$$

This reaction is slightly endothermic at room temperature. The key challenge is to avoid/substantially reduce CO formation from direct methanol decomposition and the reverse WGS reaction (RWGS) ($CO_2 + 2H_2 \rightarrow CO + H_2O$), which takes place readily under mild conditions. Thus, it is essential to develop efficient catalysts for hydrogen production from steam–methanol reformation without CO formation.

It is noted that there have been substantial works to investigate the possibility of integrating methanol decomposition to hydrogen processes (with suppressed CO content) directly with PEM fuel cells to operate a vehicle[11,12] but by and large this has not yet been successful. One technical hurdle is that the demand for power in vehicles is very high (>100 kW). As a result, a catalyst with high activity for hydrogen production at short residence time and high temperature (typically above 200 °C) is required to produce sufficient energy to supply a fuel cell vehicle with proper heat balance (ratio of water/methanol). Under such conditions, it is rather challenging to reduce the CO content in the hydrogen gas stream. In this work, we specifically seek for the application of *in-situ* catalytic reforming of methanol to supply hydrogen (and carbon dioxide) for small portable fuel cell-driven devices (0.5–100 W) that one could afford to use less-active catalyst, but still providing sufficient hydrogen for use (at lower temperature and higher water/methanol ratio), but with minimum CO content.

Thus, in this study, the direct reformation reaction has been explored at atmospheric pressure, in the temperature range 150–200 °C, and with steam to methanol molar ratios ranging from 1 to 20. The effects of reaction temperature, contact time, steam to methanol ratio and catalyst composition on methanol conversion, CO selectivity and hydrogen productivity are evaluated.

Results

Catalyst testing for steam reforming of methanol. It is important to appreciate the CO content according to equilibrium thermodynamics of the steam reforming of methanol under our reaction conditions. Theoretical calculations were thus performed to derive the equilibrium thermodynamics values (HSC Chemistry 5.11) where only the intrinsic properties of the gas species were considered. Here 1 mole of $CH_3OH_{(g)}$ and 2 moles of $H_2O_{(g)}$ were considered as the reactants, and product species of $CO_{(g)}$, $CO_{2(g)}$ and $H_{2(g)}$ were taken into account (experimentally identified). Figure 1 shows clearly that the methanol conversion can approach 100% to carbon dioxide and hydrogen at around 100 °C. But, an increase in reaction temperature particularly above 200 °C will favour CO formation (*via* the RWGS reaction). The increase in CO content will decrease the production of H_2 and CO_2 from the steam reforming of methanol and act as a poison to the downstream fuel cell catalysts. We therefore set out to develop an active and efficient catalyst for direct hydrogen production at 100–150 °C without CO formation (at least below 10 ppm) under kinetically controlled conditions.

Copper-based catalysts are well known to be active for both methanol synthesis from H_2/CO_2 and steam reforming of methanol to H_2/CO_2, presumably the key species are under micro-reversibility at different reaction conditions over the same catalytic surfaces.[5] But, the reaction mechanisms for both reactions should be compared experimentally. Figure 2 shows the comparison of various Cu-based catalysts in a fixed-bed reactor for the possible direct production of hydrogen and carbon

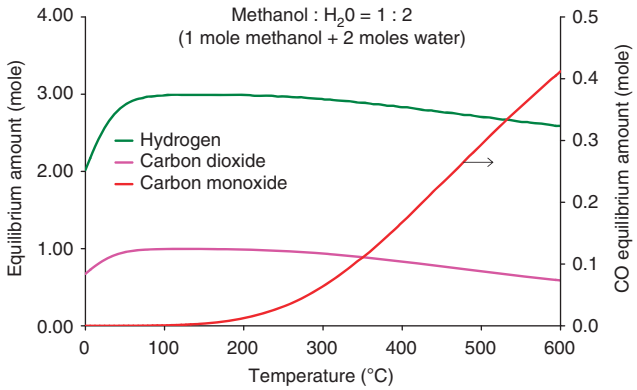

Figure 1 | Thermodynamic equilibrium product compositions. A plot of thermodynamic equilibrium product compositions as function of temperature (calculations performed with the HSC Chemistry 5.11 software).

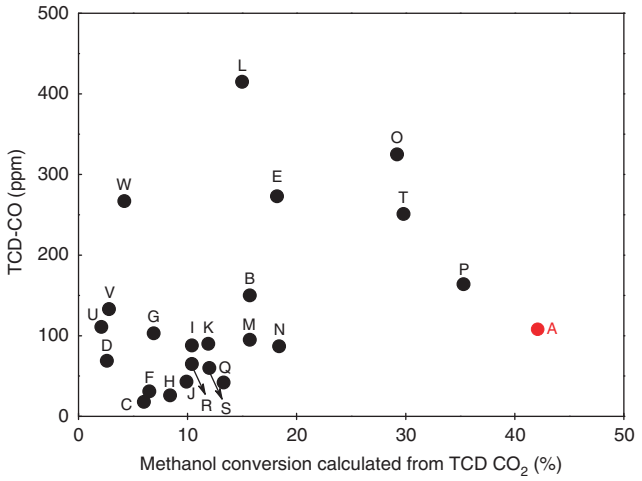

Figure 2 | Methanol conversion and CO content for typical steam-reforming reaction catalysts. (Reaction conditions: 0.40 g cat. + 0.40 g SiC; liquid feed of CH_3OH:H_2O = 1: 2 at 0.1 ml min^{-1}; N_2 carrier at 10 ml min^{-1}; 195 °C) A: 43% $CuZnGaO_x$, B: 43% $CuCeZrO_x$, C: 43% $CuZnAlO_x$, D: 43% $CuLaMnO_x$, E: 43% $CuZnO_x$, F: 43% $CuCeAlO_x$, G: 43% $CuCeGaO_x$, H: 43% $CuCeO_x$, I: 43% $CuZrO_x$, J: 43% $CuAlGaO_x$, K: 43% $CuZrGaO_x$, L: 43% $CuFeO_x$, M: 43% $CuGaO_x$, N: 43% $CuZnCeO_x$, O: 43% $CuZnZrO_x$, P: 43% $CuAlO_x$, Q: 43% $CuGaZnAlO_x$, R: 43% $CuGaCeAlO_x$, S: 43% $CuCeZnAlO_x$, T: HiFUEL R120-JM commercial catalyst.

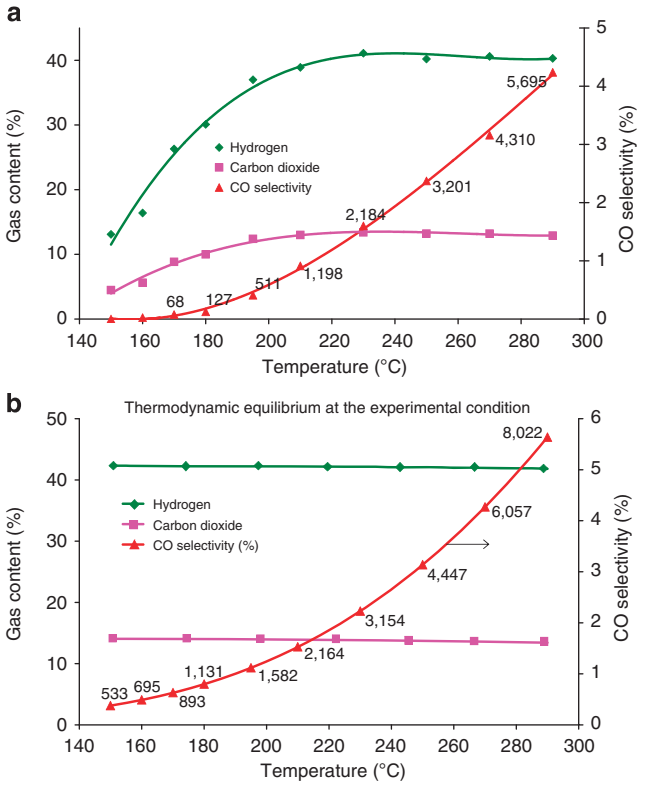

Figure 3 | Temperature-dependent catalytic performance. (**a**) A plot of catalytic performance, gas content and CO selectivity (and concentration), against reaction temperature for steam reforming of methanol by $CuZnGaO_x$; (**b**) Thermodynamic calculations (reaction conditions: 0.40 g cat. + 0.40 g SiC; liquid feed of CH_3OH:H_2O = 1: 2 at 0.01 ml min^{-1}; N_2 carrier at 10 ml min^{-1}; varying temperature).

dioxide from steam reformation of methanol at 195 °C. The H_2/CO_2 molar ratios obtained from most catalysts under these conditions were around 3:1 with low CO contents according to the stoichiometry, indicating that the steam reforming of methanol can take place under these reaction conditions. However, most catalysts were not active for the direct steam reformation of methanol (<20%) under our residence time study. Conventional catalysts $CuZnO_x$ (E), $CuZnAlO_x$ (D) and industrial Cu catalysts (T) gave either low activity or high CO content. It is interesting to note that the $CuZnGaO_x$-based catalyst (A) gave good methanol conversion but with consistently low CO content (100 ppm), which is below the thermodynamically expected values (see data below). Thus, the most active and selective $CuZnGaO_x$ catalyst was selected for further study.

Thermodynamic aspects. Figure 3a shows that above 230 °C the methanol conversion reaches close to 100%, giving a stable 3:1 H_2 to CO_2 ratio. The corresponding CO contents (selectivity) increase at increasing reaction temperature. These values agree well with the thermodynamic calculations above 230 °C, see Fig. 3b (small deviations are due to experimental errors in the substrate controls and analyses), but below this temperature it is obviously a kinetically controlled regime. Our longer contact time (W/F of 180 s kg-cat mol^{-1}) used (see Supplementary Fig. S8) allowed the Cu catalysts approaching to the equilibrium. It is noted that at 150 °C under the kinetic regime over the $CuZnGaO_x$ catalyst there was no detectable CO instead of 533 ppm. CO predicted from the theoretical calculation.

Kinetic aspects. It is also found that CO formation is not the primary product of the reaction, which is mainly derived from the RWGS. The CO content could be almost totally suppressed or severely reduced either by decreasing reaction temperature or contact time, where the slow RWGS reaction is discouraged (Supplementary Fig. S6).[11,12] It is thus clearly established that high-quality hydrogen gas production can be achieved from this low temperature non-syngas direct steam reforming (NSGDSR) over the $CuZnGaO_x$ catalyst at 150 °C with no detectable CO. The hydrogen production rate so far is measured to be 2.624 ml-H_2 min^{-1} at the 0.2 ml min^{-1} methanol–water (1:2)-feeding rate (Supplementary Figs S7 and S8). This corresponds to a hydrogen productivity of 393.6 ml-H_2 g^{-1} cat h^{-1}, the energy content of which is sufficient to support practical applications for some small mobile devices using the methanol–water as fuel without complex setup or pre- or post-treatment(s).[4] As far as we are aware, the direct catalytic conversion of methanol and water to H_2 and CO_2 at or below 150 °C, with no production of CO (not detectable at the detection limit of 1 ppm) and with usable conversion efficiencies, has not been reported before this work. This indicates the practical feasibility of the new catalytic capability for hydrogen production for small fuel cell devices.

As there appeared to give no CO formation at or below 150 °C over $CuZnGaO_x$, as shown in Fig. 3a, the next objective was to further improve the methanol conversion while keeping the CO formation at its minimum. Methanol is known to be activated by copper surface sites but it also requires catalytically active sites, presumably on a defective oxide in close proximity, for the activation of water molecules to produce active oxygen for CO_2 and H_2 formation. We have therefore re-examined the synthesis and testing of the four typical Cu catalysts very carefully in order to further reduce Cu particle sizes and enhance activities (see Methods: catalyst preparation). Table 1 shows the Cu dispersions and sizes of the four optimized Cu-based catalysts prepared from co-precipitation method after the mild reduction

Table 1 | Summary of the physical and catalytic properties of optimized Cu catalysts.

Sample	N_2 BET surface area ($m^2 g^{-1}$ cat.)	Cu dispersion (%)	Cu surface area g-cat^{-1} ($m^2 g^{-1}$ cat.)	Cu surface area g-Cu^{-1} ($m^2 g^{-1}$ Cu)	Cu particle size (nm)	CH_3OH conversion at 150 °C (%)	CO (ppm)
$CuZnO_x$	58.4	19.59	43.0	116.0	5.78	18.8	17
$CuGaO_x$	25.9	6.80	12.9	38.1	17.60	5.4	0*
$CuZnGaO_x$	79.2	30.52	65.1	178.7	3.76	22.5	0*
$CuZnAlO_x$	ND	16.71	47.3	131.9	5.09	12.6	12

Abbreviation: ND, not determined.
*No CO peak was detected by gas chromatographs, which have the lowest detection limits of 8 ppm (TCD) and 1 ppm (FID with methanator).

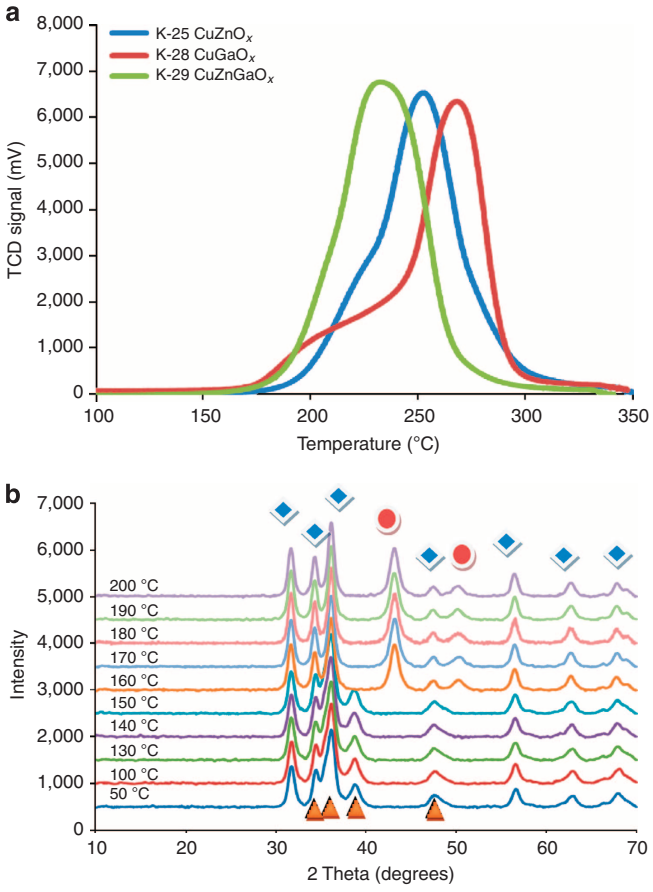

Figure 4 | TPR and XRD measurements. (**a**) TPR profiles of calcined $CuZnO_x$, $CuGaO_x$ and $CuZnGaO_x$; (**b**) *In-situ* XRD profile of $CuZnO_x$ in dilute H_2 (ZnO (blue diamonds); CuO (orange triangles); Cu (red circles)).

and corresponding methanol conversions at the methanol: water molar ratio of 1:2.

Copper analysis. There is a strong inverse correlation between Cu particle size (or Cu dispersion) and methanol-reforming activity. The promotion of catalytic activity without increasing CO content for this reaction at low temperature over $CuZnGaO_x$ clearly reflects the fast surface kinetics due to the intimate interaction of the Cu formed after reduction with the mixed oxide. It is important to characterize the catalyst for further development of this and related materials for this reaction.

The temperature-programmed reduction (TPR) technique was used to study the chemical reducibility of 'Cu-O' in the Cu-containing samples in hydrogen within the 0–500 °C range. Figure 4a displays the TPR profiles of $CuZnO_x$, $CuGaO_x$ and $CuZnGaO_x$, with broad peaks indicative of a wide distribution of 'Cu-O' species of different reducibility. Notice that a similar total peak area is obtained in all cases, showing that all the 'Cu-O' populations have been reduced completely as they all have the same atomic content of Cu (43%). It is interesting to elucidate the speciation particularly the most active 'Cu-O'species over $CuZnGaO_x$ and $CuGaO_x$. From the figure we observe the same onset reduction temperature for both $CuZnGaO_x$ and $CuGaO_x$ at ~150 °C, suggesting a similar type of 'most active Cu-O' species'. However, $CuGaO_x$ gives a higher proportion of less active 'Cu-O' that peaks at 275 °C, whereas $CuZnGaO_x$ gives a maximum at 230 °C. For $CuZnO_x$, the onset reduction temperature is at ~180 °C and reaches its maximum at 270 °C.

Corresponding *in-situ* X-ray diffraction (XRD) profiles of Cu catalysts calcined under a flowing stream of hydrogen but at longer contact time are presented in Fig. 4b and Figs 5a,b. Notice that after calcination the $CuZnO_x$ displays distinctive ZnO and CuO (excess) phases, which suggests that the intimate oxide mixture did not form a significant degree of solid solution(s) in these phases although isomorphous substitution between Cu^{2+} and Zn^{2+} (radii 0.73 and 0.74 Å, respectively) can take place in the zinc carbonate hydroxide and copper carbonate hydrate precursor (Malachite) phases to create the intimate mixture before calcination.[13] The reduction of CuO occurred at above 160 °C with the disappearance of CuO peaks and the simultaneous formation of Cu peaks. It is particularly noted that the reduction of $CuGaO_x$ and $CuZnGaO_x$ occurs at lower temperature (150 °C), before the rapid formation of large amounts of Cu phase at the expense of the CuO phase at more elevated temperatures. Thus, the incorporation of Ga^{3+} clearly promotes the reduction of some active Cu^{2+} at lower temperature: this information correlates with the lower onset reduction temperature (shoulder) at 150 °C by the TPR. In the case of $CuGaO_x$, excess CuO phase can clearly be seen after calcination but we did not detect Ga_2O_3 phase. Thus, it is likely that very small size or amorphous spinel $CuGa_2O_4$ might have originally formed during the calcination of the co-precipitated precursors. There were also no characteristic ZnO peaks in the case of $CuZnGaO_x$ but there were distinctive peaks of $ZnGa_2O_3$ (cubic spinel) and CuO. Presumably, the excess Zn^{2+} could be well dispersed on the two solid phases with a high degree of cross-substitution of $Cu^{2+}/Zn^{2+}/Ga^{3+}$ due to the similar sizes of these ions. As a result, the addition of Ga^{3+} appears to favour the formation of spinel oxide with either Cu^{2+} or Zn^{2+} possibly *via* the hydrotalcite precursors (not shown) before the calcination. At elevated temperatures the formation of Cu phase at the expense of CuO phase during reduction was again observed. From the XRD measurements of quenched samples from designated temperatures, the average Cu particle size over both $CuZnO_x$ and $CuZnGaO_x$ was found to be ca. 8 nm but the Cu size over $CuGaO_x$ was ca. 17 nm after reduction at 200 °C (Supplementary Fig. S3). It is accepted that it is essential to include Zn^{2+} in traditional methanol synthesis catalysts for textural dispersion

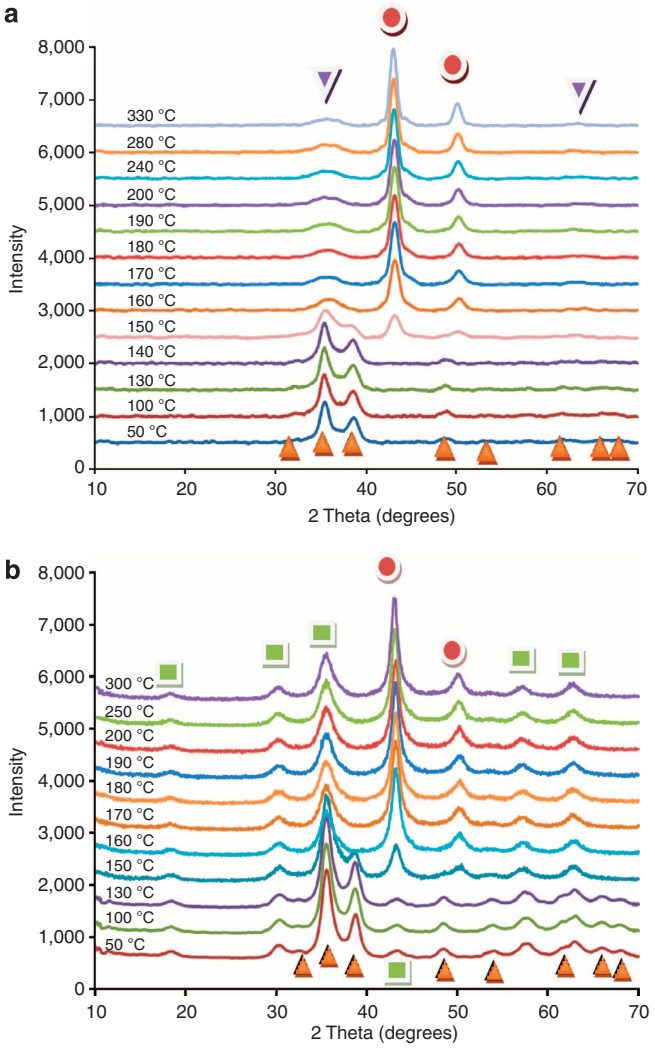

Figure 5 | XRD measurements. *In-situ* XRD profiles of (**a**) $CuGaO_x$ and (**b**) $CuZnGaO_x$ ($CuGa_2O_4$ tetragonal spinel (purple triangles); CuO (orange triangles); Cu (red circles); $ZnGa_2O_4$ cubic spinel (green squares)).

of copper phase, otherwise copper is highly susceptible to sintering.[14] Although $CuGaO_x$ shows the presence of the low temperature reduction shoulder in TPR (and *in-situ* XRD) the copper phase must have undergone a rapid sintering process to give large size particles. Notice that there is a significant discrepancy in the Cu size estimation from the N_2O measurement and XRD over these samples although XRD gives estimation on crystalline size. This is more pronounced in the case of $CuZnGaO_x$ (Table 1), even though the crystalline size estimation derived from XRD includes instrumental line-broadening effects. The large discrepancy in the apparent Cu size over $CuZnGaO_x$ measured from gas adsorption (3.76 nm) and from XRD (8 nm) indicates the formation of a large quantity of very small but active Cu clusters that had escaped XRD detection.

It is well known that spinel structure gives significant interstices and the similar sizes of $Cu^{2+}/Zn^{2+}/Ga^{3+}$ (which are same-row elements in the periodic table) are likely to cross-substitute each other to a degree at elevated temperature to give a significantly defective structure. The degree of their cross-substitution is also expected to affect the final structure, activity and stability of the material due to Jahn–Teller effect of Cu^{2+} imposed to the crystal (see Supplementary Methods). Indeed, our photoluminescence analysis clearly indicated that the $CuZnGaO_x$ gave the largest quantity of defects in the structure, dependent on the Zn:Ga ratio used. We thus suggest that a small quantity of Cu^{2+} is entrapped in the spinel phases (as non-stoichiometric excess Cu^{2+}- $CuGaO_x$ and $CuZnGaO_x$ phases, see Supplementary Methods), which is essential to generate the active copper clusters upon reduction at low temperature before the formation of larger copper particles from the extensive reduction of the frameworks CuO and $CuGa_2O_4$ at elevated temperatures. Thus, the results clearly indicate that the Ga^{3+} addition can facilitate the formation of a larger percentage of small but more active copper clusters, which give the higher activity for the methanol decomposition (Table 1).

High-angle annular dark-field scanning transmission electron microscopy (HAADF-STEM) was used to acquire a detailed microscopic view of the $CuZnGaO_x$ catalyst particles after reduction (see Methods: HADDF-STEM). Using this imaging technique, an aberration-corrected transmission electron microscope revealed a significant number of copper particles (bright contrast) in the observable thin areas of the sample. The copper-rich particles ranged in size from *ca.* 7 to 9 nm in diameter, as shown in Fig. 6a. It is interesting to see that there were very small but homogeneous copper clusters (size of 0.5–2 nm) in a close proximity to the large Cu particles. Energy-dispersive X-ray spectroscopy confirmed that they were richer in Cu than the background, although the Cu content could not be unambiguously determined due to the resolution limit of the equipment.

To analyse the small Cu particles/clusters within the $CuZnGaO_x$ catalyst in further detail, we employed atom probe tomography (APT).[4] As shown in Fig. 6b, by examination of the Cu density isosurface map we detected some clearly-defined Cu particles with sizes in the diameter range of 4–8 nm (composed of nearly 100% Cu as revealed from the mass spectroscopy). A typical atom map from the APT analysis, shown in Fig. 6c indicates that there were also very small Cu-rich regions (that is region A). A closer examination of the copper atoms distribution in the region A clearly reveals the small copper-rich area (copper clusters) of ca. 0.4–0.8 nm with 0.5 nm as the most probable mean size (Fig. 6d), which contained exclusively the Cu signal from mass spectroscopic analysis (Fig. 6e). Thus, the direct visualization by both the HADDF-STEM and APT discloses the bimodal distribution of large copper particles (from reduction of CuO and solid frameworks) together with very small copper clusters (from Cu^{2+} in spinel interstices). In addition, XPS also confirms that there were two differentiable binding energy, BE of Cu 2p 3/2 peaks, one of a typical Cu phase at 932.4 eV and the other at 934.2 eV attributed to small copper clusters (Supplementary Fig. S4).[15] It is thus evident that the small copper clusters on defective oxide support produced from the reduction of copper ions entrapped in the spinel phase are responsible for the high activity in steam–methanol conversion to hydrogen and carbon dioxide at 150 °C.

Discussion

The *in-situ* catalytic production of hydrogen by steam reforming of methanol is an attractive option for use in decentralized production of clean electrical energy from PEM fuel cells. Present technologies for methanol reformation including steam reforming, partial oxidation and their combination *via* the syngas route suffer from problems that would require cumbersome CO cleanups, which in turn would lead to severe degradation in fuel cells performance. Also, there is insufficient room for such operations in portable fuel cell consumer products. Here we report a NSGDSR route at <200 °C that can integrate the

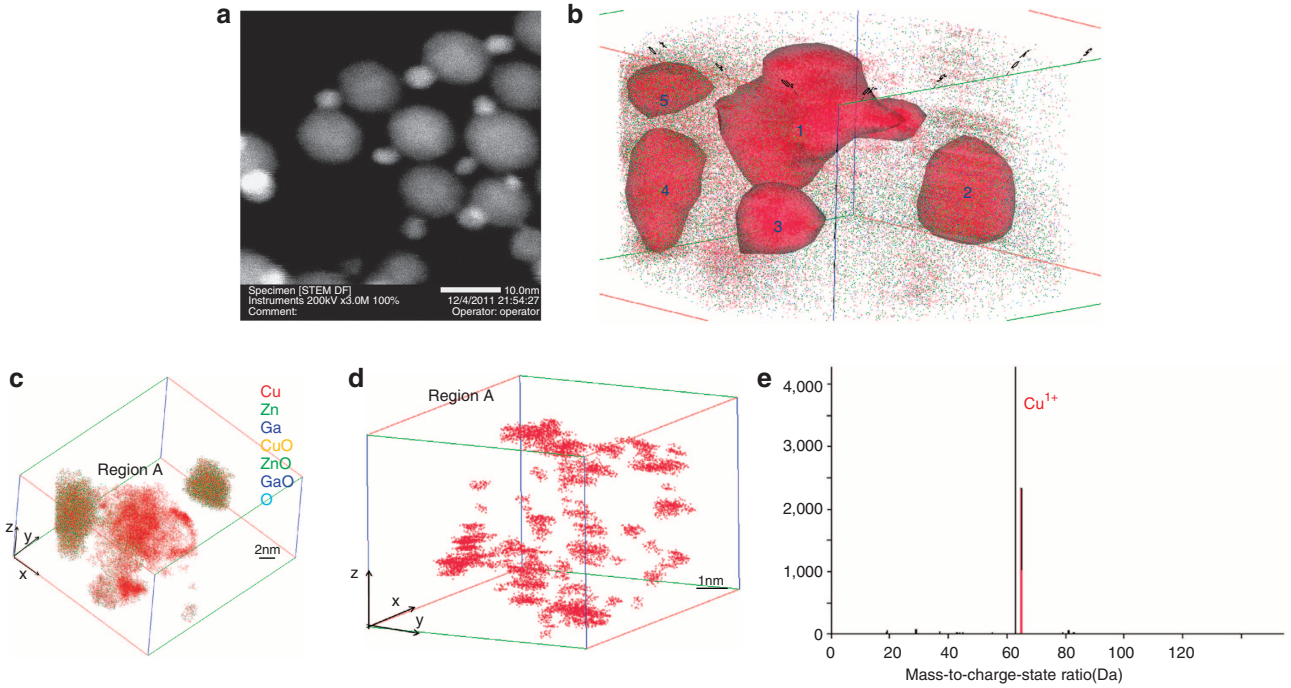

Figure 6 | Atomic distribution within the particles. (**a**) HAADF-STEM imaging of $CuZnGaO_x$ catalyst after reduction showing bimodal distribution of large Cu particles (7–9 nm) and small Cu clusters (0.5–2 nm). (**b**) APT data of the specimen after reduction showing Cu particles (4–8 nm) and high-density Cu cluster areas in the solid matrix (red patches). (**c**) Atom map of small Cu-rich areas; scale bar: 2 nm. (**d**) Detailed Cu distribution in region A; scale bar: 1 nm. (**e**) Cu signal from the region A identified by mass spectroscopy.

endothermic methanol steam reforming with the exothermic heat generated from the PEM fuel cells, which may offer good heat transfer characteristics. In addition, blending oxygen/air into NSGDSR to encourage combustion may also balance the total thermodynamic requirements of this system. The important finding from this work is that under these reaction conditions, no CO formation (below 1 ppm detection limit) is observed, whereas usable conversion of methanol to CO_2/H_2 over $CuGaZnO_x$ can be achieved. Thus, this new route is technically feasible and can deliver a high quality of hydrogen gas for small mobile fuel cell devices. We have identified an active type of catalyst basing on $CuGaZnO_x$ that can deliver high activity and selectivity for hydrogen production from the NSGDSR route. It has been reported in the literature that Ga^{3+} can promote hydrogenation activity of CO_2 to methanol over Cu/ZnO[7,8] and also hydrogenolysis of glycerol in water by stabilizing the copper phase on the catalysts.[16] Our evidence clearly suggests that Ga^{3+} incorporation in Cu/ZnO system produces the formation of a Cu^{2+}-containing spinel phase, from which a high population of ultrafine copper clusters can be generated and stabilized during reduction at low temperature (see Supplementary Methods and Supplementary Fig. S5). The higher methanol steam reformation activity could be due to the presence of small copper islands under high isomorphic strain on the support[17,18] or to the structure or morphology of the catalyst giving optimum balance between metallic Cu^0 and Cu^1 for maximum activity and selectivity.[12] The long-term stability of these surface copper clusters stabilized by gallium during catalysis is not yet known, but the working catalyst appears to be stable for at least a few days under our testing conditions. A recent report suggests the highly active stepped copper particles could be decorated with heteroatoms (Zn atoms) in the industrial $Cu/ZnO/Al_2O_3$ catalyst.[19] It would be interesting to investigate whether Ga or Zn atoms stabilize the small copper clusters in the reduced $CuGaZnO_x$ catalyst. Overall, the NSGDSR process can provide a high quality of *in-situ* hydrogen gas at lower temperature from methanol–water mixture. Further optimization in the content of these surface supported copper clusters from the Cu^{2+}-rich-spinel structures is on-going.

Methods

Catalyst preparation. All copper-based catalysts were synthesized using a pH-controlled co-precipitation method. The precursors were hydrated metal nitrate salts typically: $Cu(NO_3)_2 \cdot 3H_2O$, $Zn(NO_3)_2 \cdot 6H_2O$ and $Ga(NO_3)_3 \cdot 9H_2O$ (Aldrich), each of which was dissolved completely in 100 ml de-ionized water (Supplementary Table S1).

The initial catalyst (catalysts presented in Fig. 2) was prepared *via* a simple co-precipitation method. The precursor metal nitrate salts were dissolved and combined in 100 ml DI water, followed by a drop-wise addition of aqueous Na_2CO_3 (3.50 g in 100 ml DI water) used to produce the precipitate. Both solutions were added at about 0.05 ml s^{-1} by a dropper to a round-bottomed flask containing 300 ml DI water and a magnetic stirring bar maintained at 1,500 rpm, and heated to 80–90 °C with pH controlled between 6 and 7. The resulting precipitate was aged in solution at this temperature for 24 h. After ageing, the precipitate was centrifuged 6–12 times at 6,000 rpm for 5 min and washed with 50 ml DI water between each period to remove Na^+ ions. The resulting solid was powdered, then dried in air at 80–100 °C overnight and subsequently calcined in static air at 3 °C min^{-1} up to 380 °C for 180 min to produce the catalyst. It was later found that the activity of catalyst is very sensitive to precise value of the pH used and the speed of dropping one solution to another. As a result, for optimized catalyst (catalyst presented in Table 1), the pH of the precipitating solution was carefully maintained at 6.5 by adding a Na_2CO_3 aqueous solution (prepared by dissolving 3.50 g of Na_2CO_3 in 100 ml DI water). A delivery pump and two 50 ml syringes were used to inject the precursor metal nitrate solution at the constant rate of 0.42 ml min^{-1} in an automatic and reproducible manner. The Na_2CO_3 solution was added using a high-performance liquid chromatography (HPLC) pump at the rate of 0.5–1.0 ml min^{-1}. The solutions were added simultaneously into a plastic reactor containing 250 ml of pre-heated DI water and a magnetic stirring bar maintained at 1,200 rpm. The precipitation process took place at around 80 °C, with the oil bath set at 100 °C. The pH was measured using a temperature-dependent pH metre and was controlled between pH 6 and 7, with an error range of ± 0.1. Once the addition of the precursor metal nitrate solution was completed, the pH was measured again to ensure that the target pH has been proper reached before putting on the lid of the reactor. The resulting precipitate was aged in solution at 80 °C, for 15 h. After ageing the precipitate was extracted by centrifugation at 4,000 rpm. The centrifuged precipitate was then washed with DI

water 3 times at 3,000 rpm for 10 min in order to remove Na^+ ions. The resulting wet solid was dried in air at 78 °C overnight and then calcined in static air at 3 °C min^{-1} up to 380 °C for 3 h to produce the final optimized catalyst for testing (Supplementary Fig. S1).

TPR. TPR measurements were obtained using a ThermoQuest TPRO 110 instrument. Inside the TPR quartz tube, 0.026 g of the calcined catalyst sample was sandwiched between two layers of glass wool with a thermocouple placed in contact with the sample. The TPR tube was then inserted into the instrument for a helium pretreatment. The helium gas pretreatment (He running through the TPR tube at 10 ml min^{-1} at a temperature ramp of 10 °C min^{-1} from 40 °C up to 150 °C, then held for 5 min before cooling) cleaned the catalyst surface by removing any absorbed ambient gas molecules. After the pretreatment, a reduction treatment (5% H_2 in Argon flowing through the TPR tube at 20 ml min^{-1} at a temperature ramp of 10 °C min^{-1} from 40 °C up to 330 °C, then held at 330 °C for 30 min before cooling down to room temperature) was carried out to reduce the Cu^{2+} within the sample. Cu(II)O was reduced to Cu(0) by the flow of hydrogen gas in the reduction treatment. The consumption of hydrogen gas changed the conductivity of the gas stream; hence, the change in conductivity was measured and calibrated as a function of both temperature and time to produce the TPR profile.

Chemisorption. The reduction treatment of Cu^{2+} to Cu^0 in the catalyst sample (1st TPR) was followed by N_2O chemisorption at room temperature, to determine the size of copper metal particles. Treatment with 5% N_2O/Ar at 20 ml min^{-1} for 40 min was carried out to re-oxidise only the Cu surface *via* dissociative chemisorption. To remove any remaining adsorbed N_2O, another He pretreatment (He flowing at 10 ml min^{-1} for 10 min at RT) was carried out. This was followed by a second reduction treatment (2nd TPR: 5% H_2 in Argon at 20 ml min^{-1} at a temperature ramp of 10 °C min^{-1} from 40 °C up to 330 °C). By analysing data from the first and second TPR, it was possible to determine the Cu surface area of the catalyst sample by precalibrating the TPR with a Cu(II)O standard of known Cu content. Standard samples of Cu(II)O: 0.005, 0.0010 and 0.0015 g (Aldrich) were used to perform the TPR and the number of moles of hydrogen consumed was calculated. The result was then plotted against the TPR-integrated peak area to give a first-order calibration plot. Supplementary Figure S2 shows the correlation between TPR peak area and H_2 consumption.

***In-situ* XRD**. *In-situ* XRD for programmed reduction was conducted in the temperature range 30–330 °C. Ten microgram of sample was placed onto a quartz plate under a flowing stream of 10 ml min^{-1} of 5% H_2 in argon in an *in-situ* cell with a longer contact time than those of the TPR experiments. The XRD profile was collected by a Philips PW-1729 diffractometer with Bragg-Brentano focusing geometry using $Cu_{K\alpha}$ radiation ($\lambda = 1.5418$ Å) from a generator operating at 40 kV and 40 mA.

HAADF-STEM. Bright field imaging and HAADF-STEM were both used to investigate the structure of the Cu-based catalyst materials after reduction. Using these imaging techniques, an aberration-corrected transmission electron microscope can reveal small Cu particles with a high contrast (bright spots) from the background.

APT. Cu-containing catalyst nanoparticles were deposited onto preformed, needle-shaped Pt-Rh atom probe specimens, themselves electropolished in a molten salt mixture (4:1 $NaNO_3$: NaCl) starting from platinum–22at% rhodium wire (0.1 mm dia, Alfa-Aesar). Using stock solutions of nanoparticles in methanol, a droplet was placed in a gold electropolishing loop and a voltage bias applied between the loop and the Pt–Rh specimen. On dipping the needle into the loop, nanoparticles were drawn through the potential gradient by electrophoresis towards the apex region, where they subsequently attached. Each sample was then inspected in a transmission electron microscope (TEM), (Phillips CM20) to confirm nanoparticle deposition. The variables of particle type, size and polarity, along with specimen sharpness and dipping duration all affect the deposition process, and had to be carefully explored. Exposing the specimens for longer periods in the nanoparticle solution allowed further deposition, but the larger degree of agglomeration of particles was difficult to analyse at later time. Typical conditions to deposit a thin layer of Cu nanoparticles were 5–15 V, applied for ~10 s of total current flowing, using a Pt–Rh needle of ~40–50 nm end radius. Once deposited and checked in the TEM, each sample was transferred to the storage chamber (Cameca LEAP 3000HR) to minimize contamination. Samples were analysed for APT using a pulsed laser mode (0.45 nJ energy, 10 µm spot size, 160 kHz repetition rate) at a specimen base temperature of 55 K.

XPS. After reduction, samples were carefully transferred in a glove bag without air exposure and analysed by XPS. Supplementary Figure S4 shows a typical survey scan of $CuZnGaO_x$ and the binding energy for the Cu 2p 3/2 peak before and after reduction.

References

1. Zhao, T.S *Microfuel Cells: Principles and Applications* (Elsevier, USA, 2009).
2. Van den Berg, A. W. C. & Arean, C. O. Materials for hydrogen storage: current research trends and perspectives. *Chem. Commun.* **44,** 668–681 (2008).
3. Springer, T. E., Rockward, T., Zawodzinski, T. A. & Gottesfeld, S. Model for polymer electrolyte fuel cell operation on reformate feed: effects of CO, H2 dilution, and high fuel utilization. *J. Electrochem. Soc.* **148,** A11–A23 (2001).
4. Tedsree, K. *et al.* Hydrogen production from formic acid decomposition at room temperature using a Ag–Pd core–shell nanocatalyst. *Nat. Nanotechnol.* **6,** 302–307 (2011).
5. Olah, G. A., Coeppert, A. & Prakash, G. K. S. *Beyond Oil and Gas: The Methanol Economy*. 2nd edn. (Wiley-VCH, Los Angeles, CA, USA, 1998).
6. Sun, Hsiang-Ning (Exxon Mobil). Patent. One step conversion of methanol to hydrogen and carbon dioxide. WO98/29333/PCT/US97/24124 (1998).
7. Toyir, J., Ramírez de la Piscina, P., Fierro, J. L. S. & Homs, N. Highly effective conversion of CO_2 to methanol over supported and promoted copper-based catalysts: influence of support and promoter. *Appl.Catal. B: Env.* **29,** 207–215 (2001).
8. Saito, M., Fujitani, T., Takeuchi, M. & Watanabe, T. Development of copper/zinc oxide-based multicomponent catalysts for methanol synthesis from carbon dioxide and hydrogen. *Appl. Catal. A Gen.* **138,** 311–318 (1996).
9. Słoczynski, J. *et al.* Effect of metal oxide additives on the activity and stability of $Cu/ZnO/ZrO_2$ catalysts in the synthesis of methanol from CO_2 and H_2. *Appl. Catal. A: Gen.* **310,** 127–137 (2006).
10. Liao, F. *et al.* Morphology-dependent interactions of ZnO with Cu nanoparticles at the materials' interface in selective hydrogenation of CO_2 to CH_3OH. *Angew Chem. Int. Ed.* **123,** 2210–2213 (2011).
11. Purnama, H. *et al.* CO formation/selectivity for steam reforming of methanol with a commercial CuO/ZnO/Al2O3 catalyst. *Appl. Catal. A* **259,** 83–84 (2004).
12. Ritzkopf, I., Vukojević, S., Weidenthaler, C., Grunwaldt, J.D. & Schüth, F. Decreased CO production in methanol steam reforming over Cu/ZrO2 catalysts prepared by the microemulsion technique. *Appl. Catal. A* **302,** 215–223 (2006).
13. Shen, G. C., Fujita, S. I., Matsumoto, S. & Takezawa, N. Steam reforming of methanol on binary CuZnO catalysts: Effects of preparation condition upon precursors, surface structure and catalytic activity. *J. Mol. Catal. A Chem.* **124,** 123–136 (1997).
14. Palo, D. R., Dagle, R. A. & Holladay, J. D. Methanol steam reforming for hydrogen production. *Chem. Rev.* **107,** 3992–4021 (2007).
15. Crescenzi, M. D., Diociaiuti, M., Lozzi, L., Picozzi, P. & Santucci, S. Size effects on the linewidths of the Auger spectra of Cu clusters. *Surface Sci.* **178,** 282–289 (1986).
16. Bienholz, A., Blume, R., Knop-Gericke, A., Girgsdies, F., Behrens, M. & Claus, P. Prevention of catalyst deactivation in the hydrogenolysis of glycerol by Ga_2O_3-modified copper/zinc oxide catalysts. *J. Phys. Chem. C* **115,** 999–1005 (2011).
17. Kasatkin, I., Kurr, P., Kniep, B., Trunschke, A. & Schlögl, R. Role of lattice strain and defects in copper particles on the activity of $Cu/ZnO/Al_2O_3$ catalysts for methanol synthesis. *Angew Chem. Int. Ed.* **46,** 7324–7327 (2007).
18. Ressler, T., Kniep, B. L., Katsatkin, I. & Schlogl, R. The microstructure of copper zinc oxide catalysts: bridging the materials gap. *Angew Chem. Int. Ed.* **44,** 4704–4707 (2005).
19. Behrens, M. *et al.* The active site of methanol synthesis over $Cu/ZnO/Al_2O_3$ industrial catalysts. *Science* **336,** 893–897 (2012).

Acknowledgements

This work was funded by EPSRC, UK. We thank Dr Jingping Hu and Prof. John Foord of Oxford Chemistry for support of the XPS characterization and Prof. Heyong He of Fudan University, China for the HAADF-STEM characterization. We also thank Drs Martin Fowles and Colin Park of Johnson Matthey Billingham, UK for useful discussion. W.T. would like to thank China Scholarship Committee (CSC) and the permission from the ECUST to undertake some of the research at Oxford University.

Author contributions

K.M.K.Y., W.T., A.W. and K.C. contributed to material synthesis, testing and characterization. T.L. and G. S. contributed to APT characterization. S.C.E.T. initiated, supervised and coordinated this research. All authors contributed to the discussions of the results in this manuscript.

Additional information

Supplementary Information accompanies this paper on http://www.nature.com/naturecommunications

Competing financial interests: The authors declare no competing financial interests.

Reprints and permission information is available online at http://npg.nature.com/reprintsandpermissions/

How to cite this article: Yu K.M.K. *et al.* Non-syngas direct steam reforming of methanol to hydrogen and carbon dioxide at low temperature. *Nat. Commun.* 3:1230 doi: 10.1038/ncomms2242 (2012).